Structural and dynamical quality assessment of gap-filled sea surface temperature products

Earth and Space Science

RESEARCH ARTICLE
10.1029/2023EA003088

Structural and Dynamical Quality Assessment of Gap-Filled Sea Surface Temperature Products

Cristina González-Haro[1,2], Jordi Isern-Fontanet[1,2], Antonio Turiel[1,2], Christopher J. Merchant[3], and Peter Cornillon[4]

[1]Department of Physical Oceanography, Institut de Ciències del Mar, CSIC, Barcelona Expert Center on Remote Sensing, Barcelona, Spain, [2]Institut Català de Recerca per a la Governança del Mar, Barcelona, Spain, [3]Department of Meteorology, National Centre for Earth Observation, University of Reading, Reading, UK, [4]Graduate School of Oceanography, University of Rhode Island, Narragansett, RI, USA

Key Points:

- We proposed a new diagnostic to assess the structural and dynamical properties of sea surface temperature (SST) products
- This diagnostic is based on multifractal theory of turbulence and consists computing the singularity spectrum
- The different schemes used to produce gap-filled SST products may contribute to the loss of dynamical information or structural coherence

Correspondence to:
C. González-Haro,
cgharo@icm.csic.es

Citation:
González-Haro, C., Isern-Fontanet, J., Turiel, A., Merchant, C. J., & Cornillon, P. (2024). Structural and dynamical quality assessment of gap-filled sea surface temperature products. *Earth and Space Science*, *11*, e2023EA003088. https://doi.org/10.1029/2023EA003088

Received 13 JUN 2023
Accepted 2 JUL 2024

Author Contributions:
Conceptualization: Cristina González-Haro, Jordi Isern-Fontanet
Data curation: Cristina González-Haro
Formal analysis: Cristina González-Haro, Antonio Turiel, Christopher J. Merchant, Peter Cornillon
Funding acquisition: Antonio Turiel
Investigation: Cristina González-Haro, Jordi Isern-Fontanet, Antonio Turiel, Christopher J. Merchant, Peter Cornillon
Methodology: Jordi Isern-Fontanet, Antonio Turiel
Resources: Jordi Isern-Fontanet, Antonio Turiel
Software: Cristina González-Haro, Jordi Isern-Fontanet
Writing – original draft: Cristina González-Haro
Writing – review & editing: Jordi Isern-Fontanet, Antonio Turiel, Christopher J. Merchant, Peter Cornillon

Abstract Previous studies that intercompared global Level-4 (L4) sea surface temperature (SST) analyses were centered on the assessment of the accuracy and bias of SST by comparing them with independent near-surface Argo profile temperature data. This type of assessment is centered on the absolute value of SST rather than on SST spatial properties (gradients), which is more relevant to the study of oceanographic features (e.g., fronts, eddies, etc.) and ocean dynamics. Here, we use, for the first time, the spectrum of singularity exponents to assess the structural and dynamical quality of different L4 gap-filled products based on the multifractal theory of turbulence. Singularity exponents represent the geometrical projection of the turbulence cascade, and its singular spectrum can be related to the probability density function of the singularity exponents normalized by the scale. Our results reveal that the different schemes used to produce the L4 SST products generate different singularity spectra, which are then used to identify a potential loss of dynamical information or structural coherence. This new diagnostic constitutes a valuable tool to assess the structural quality of SST products and can support data satellite SST producers efforts to improve the interpolation schemes used to generate gap-filled SST products.

Plain Language Summary Gap-filled sea surface temperature (SST) gridded products are generated by combining satellite and, in some cases, in situ observations. Previous studies intercomparing the different SST products focused on assessing the differences between the SST products and in situ observations. However, what is relevant for ocean dynamics studies is the local spatial differences of the SST fields. In this work, we propose a new diagnostic that allows us to assess the dynamical quality of SST products. This new diagnostic is based on the multifractal theory of turbulence and enables the identification of the regions where the SST fields do not properly describe ocean dynamics. This diagnostic is a valuable tool that can help the data satellite SST producers to improve the way the different observations are blended in order to build SST fields that are more dynamically coherent.

1. Introduction

Sea surface temperature (SST) plays a key role in the understanding, monitoring and prediction of heat, freshwater and momentum flux exchanges at the ocean-atmosphere interface. Changes of SST force small and large-scale changes in the atmospheric boundary layer–and above–on seasonal, decadal and climatic timescales (O'Neill et al., 2010; Perlin et al., 2014; Renault et al., 2019). Because of the important role it plays in climate (Deser et al., 2010) it has been designated an Essential Climate Variable used to monitor, predict and assess the impact of climate change. SST is also required as a boundary condition for ocean, weather and climate forecasting models (Chelton & Wentz, 2005; Robinson et al., 2012). Therefore, having accurate SST data is essential from operational to climate applications.

SST has been monitored since mid-1850s (Rayner et al., 2006). Observations are obtained from various in situ platforms including moored and drifting buoys, Argo floats and ships of opportunity. Global and synoptic observation of SST is only feasible from earth-observation satellites (O'Carroll et al., 2019). The Group for High Resolution Sea Surface Temperature (GHRSST; www.ghrsst.org; Donlon et al., 2009) is a self-organizing group of international researchers and operational practitioners aiming to coordinate the provision of SST products developed and distributed by different agencies and research institutes. During the past decade, the GHRSST community has strongly encouraged the development of high spatial resolution gap-free SST data and analysis products to satisfy the need of users. These GHRSST formatted Level-4 (L4) SST products combine multiple

satellite SST observations from multiple sensors/platforms, usually also including in situ observations (Beggs, 2010; Donlon et al., 2009). However, the different interpolation schemes and related configurations used to blend SST observations induce significant differences between L4 SST products (Dash et al., 2012; Martin et al., 2012). The assessment and intercomparison of SST L4 products is key for data providers to improve their algorithms and for users to select the best product for their applications. GHRSST provides users with some guidelines identifying the most important issues they need to consider when choosing a SST product (Beggs, 2021; GHRSST Project Office et al., 2023) but the difficulty of finding and then choosing the appropriate product is still seen as a major obstacle by many in the user community.

Several intercomparisons of L4 SST products have been performed (Dash et al., 2012; Fiedler, McLaren, et al., 2019; Martin et al., 2012; Woo & Park, 2020; Yang et al., 2021). Most of these focused on assessing the performance in terms of accuracy, bias and the spatial homogeneity using near-surface Argo data that many GHRSST data producers reserve specifically for product assessment. Other assessments have focused on the spatio-temporal variability, and more specifically, on the extended observation of SST alterations, such as long-term trends, concluding that most of the L4 data sets are compatible with climate applications (Yang et al., 2021). However, this type of assessment is focused on the accuracy, the absolute value, of SST rather than on its precision. It is the latter that is of importance in most studies of ocean features (e.g., fronts, gradients, eddies) and of ocean dynamics, especially at the submesoscale. Feature resolution, or the effective spatial resolution of a product, is not necessarily related to grid resolution and is generally quantified using spectral analysis (Reynolds et al., 2013) or scale analysis (Skákala et al., 2019). Fiedler, Mao, et al. (2019) used spectral analysis in the Gulf Stream region to show that the new flow-dependent formulation, they proposed, contributed to an improvement of the effective spatial resolution, while Yang et al. (2021) examined the spectral content of SST fields in the equatorial Pacific for several L4 SST data sets in order to ensure that the interpolation to a 1° common grid did not compromise the interpretation of the long-term temporal variability diagnosis. Fiedler, McLaren, et al. (2019) and Martin et al. (2012) approached feature intercomparison via a qualitative comparison of the horizontal SST gradients. It is difficult to provide a quantitative metric for the quality of SST gradients because of the lack of a sufficiently large set of in situ observations with which to compare these gradients, although very recent works have tackled this issue at a regional scale: Wick et al. (2023) for the northwest tropical Atlantic, and Koutantou et al. (2023) for the Arctic Ocean and Alaskan coastal waters.

Research related to L4 fields falls into two categories: studies undertaken to evaluate the quality of the data sets and those focusing on the use of these data sets to address oceanographic problems. The latter may be further subdivided into those addressing large scale–100+ kms–and those undertaking studies at the meso- and submesoscale. In the following we provide a brief overview of these studies. Of significant interest with regard to processes at the submeso- to mesoscale are studies of fully developed turbulence, studies generally requiring spatially dense SST fields. Progress in this area since the early geometric approach of Meneveau, Sreenivasan, and collaborators (Meneveau & Sreenivasan, 1991; Sreenivasan, 1991) has been slow, in part due to some technical limitations such as the lack of computational resources and the relatively poor quality of earlier L4 fields.

The validity of the multifractal framework has been evaluated for the oceans in multiple studies (e.g., among others Lovejoy et al., 2001; Seuront & Stanley, 2014; Turiel et al., 2005). For SST, Isern-Fontanet et al. (2007) confirmed that satellite observations present multifractal structures, implying that the multifractal formalism can be applied to SST observations to extract properties of the underlying flow. And, later, Isern-Fontanet et al. (2022) applied this framework to uncover how the intensity of the strongest fronts contribute to the global statistical properties of SST. Here, we take a step forward and use the multifractal theory of turbulence to assess different SST products from a dynamical and structural perspective, focusing on the representation of the energy cascade of turbulence. The paper is organized as follows: Section 2 puts the multifractal theory of turbulence in the context of oceanography; Section 3 describes the assessed SST data sets and Section 4 the algorithms used for this study; Sections 5 and 6 describe the results and discuss them, respectively; and finally, Section 7 summarizes the conclusions.

2. Theoretical Framework

Coarse grained SST gradients are constructed by low-pass filtering the magnitude of the thermal gradient as

$$\overline{|\nabla T|}_{\ell}\left(\vec{x}\right) \equiv \int_{\mathbf{R}^d} \ell^{-d} G\left(\ell^{-1}\vec{y}\right) |\nabla T|\left(\vec{x}+\vec{y}\right) d\vec{y}, \tag{1}$$

where $\vec{x}$ is the position vector, $d = 2$ is the dimension of the embedding space (2 in this case, as we deal with images); ℓ is the scale of the filter $G(\vec{x})$, which is a normalized positive function with fast decay to zero as $|\vec{x}| \to \infty$; $T(\vec{x})$ is SST and $\nabla = (\partial_x, \partial_y)$ is the gradient operator (Eyink, 2005; Turiel et al., 2008). At small enough scales, coarse grained thermal gradients can be approximated by the dominant term of a generalized Taylor series as in Arneodo et al. (1995) and Muzy et al. (1994), which is given by

$$\overline{|\nabla T|}_{\ell}(\vec{x}) \sim \left(\frac{\ell}{\ell_0}\right)^{h(\vec{x})}, \tag{2}$$

where $\ell_0 \gg \ell$ is the integral scale of the flow. The scaling exponents $h(\vec{x})$, known as singularity exponents, are a generalization of Hölder exponents and quantify the degree of continuity of SST around the point $\vec{x}$. Indeed, if $h(\vec{x}) \in (n, n+1)$ with n being a positive integer, $\overline{|\nabla T|}_{\ell}(\vec{x})$ is differentiable n times but not $n+1$ (Arneodo et al., 1995). Recall that singularity exponents of gradients can be negative, that is, gradients can contain singularities (Frisch, 1995). This way of locally characterizing the regularity of the function at each point constitutes the basis of the so-called Multifractal Microcanonical Formalism (MMF), which is not only capable of determining the local scaling exponent at each point, but also of providing insights about the geometry of the flow (Turiel et al., 2008). From an oceanographic point of view, singularity exponents can be interpreted as a measure of the steepness of the front, with the most abrupt fronts being those with the smallest values of h (Isern-Fontanet et al., 2022).

The inner organization of the turbulent flow provided by the singularity exponents can be used to divide the oceanic region under study into subsets according to the common values of singularity exponents, namely:

$$F_{h_0} \equiv \left\{\vec{x} \mid h(\vec{x}) = h_0\right\}, \tag{3}$$

where the fractal components F_h define a hierarchy of sets that is intimately related to the statistical properties of the flow and particularly to the turbulent cascade (Isern-Fontanet & Turiel, 2021). To partition the oceanic region into subsets, we define the singularity spectrum, which is a concave function of h according MMF (Frisch, 1995), as the fractal dimensions of the different fractal components F_h, that is:

$$D(h_0) \equiv d_F\left(F_{h_0}\right) = d_F\left(\left\{\vec{x} \mid h(\vec{x}) = h_0\right\}\right), \tag{4}$$

where $d_F(A)$ is the fractal dimension of set A.

It follows that the singularity spectrum $D(h)$ is a statistical feature of the multifractal structure as it completely defines the statistical properties of the cascade process. Roughly speaking, $D(h)$ characterizes the "volume" occupied by the fronts with intensity h. As the singularity components F_h are of fractal character, the distribution of singularity exponents $\rho(h)$ at a given observation scale behaves as:

$$\rho(h) \sim \left(\frac{\ell}{\ell_0}\right)^{d-D(h)}, \tag{5}$$

where, as above, $\ell/\ell_0 \to 0$ Pont et al. (2013). Moreover, the singularity spectrum $D(h)$ can also be related to the more classical approach to turbulence through the scaling exponents of the structure functions of temperature (e.g., Isern-Fontanet et al., 2022).

3. Data

We intercompare five SST data sets, four of which combine observations from different satellites, and in some cases in situ temperature measurements, to generate daily gap-free (L4, optimally interpolated for these data sets) global SST fields. We have also included a single sensor Level-3 (L3) data set that has a 3 days temporal

Table 1
Descriptive Comparison Summary for the Sea Surface Temperature (SST) Products Described in Section 3

Data set	Institute, Country	Level	Product version	Observation input	Horizontal spacing grid	Main reference
SST_AMSR2_REMSS	Remote Sensing Systems, USA	L3	8.2	MW	0.25° × 0.25°	Wentz et al. (2021)
SST_CMC	Canadian Meteorological Center, Canada	L4	3.0	IR + MW + in situ	0.21° × 0.1°	Brasnett (2008)
OSTIA	Met Office, UK	L4	2.0	IR + MW + in situ	0.05° × 0.05°	Good et al. (2020)
SST_CCI	Met Office, UK (ESA SST CCI project)	L4	2.1	IR	0.05° × 0.05°	Merchant et al. (2019)
SST_MUR	Jet Propulsion Laboratory, USA	L4	4.1	IR + MW + in situ	0.01° × 0.01°	Chin et al. (2017)

Note. All data sets have a daily temporal resolution, but the SST_AMSR2_REMSS with a 3 days temporal resolution. Input observations are derived from satellite Infrared (IR) and/or microwave (MW) sensors.

resolution to increase global coverage. The intercomparison of the SST products is performed for 2016. We describe below the main characteristics of the SST products used in this study (for a summary description see Table 1). Given the number of sensors, the satellites carrying these sensors, the resulting L4 products and the organizations flying these sensors and/or producing the data products, with the exception of their occurrence in subsection titles, we expand the associated acronyms in the acronym list at the end of this document rather than in the body of the text.

3.1. Remote Sensing Systems (REMSS)

The second generation Advanced Microwave Scanning Radiometer 2 (AMSR2) was launched in 2012, on the Japanese satellite "Shizuku" (Global Change Observing Mission—Water [GCOM-W1]; Heygster et al., 2017; Kachi et al., 2017). The 3-day averaged AMSR2 data (v8.2) with a grid spacing of 0.25° were used in this study because of their relatively complete global coverage. The data set, produced by Remote Sensing Systems and sponsored by the NASA AMSR-E Science Team, can be downloaded from REMSS's web site: https://data.remss.com/amsr2/ocean/L3/, accessed on 11 August 2022. For more details please refer to Wentz et al. (2021).

3.2. Canadian Meteorological Center (CMC)

The Canadian Meteorological Center (CMC) generates a daily operational analysis of SST at L4, adhering to GHRSST standards. This analysis incorporates Infrared (IR) satellite data from Advanced Very High Resolution Radiometer (AVHRR) instruments on National Oceanic and Atmospheric Administration (NOAA)-18, NOAA-19, Meteorological Operational satellite-A, and Meteorological Operational satellite-B, along with microwave (MW) data from AMSR2 on the GCOM-W1 satellite. Additionally, in situ SST observations from drifting buoys and ships in the International Comprehensive Ocean-Atmosphere Data Set program are used. Statistical interpolation techniques are employed to refresh the global grid analysis with a 0.1° resolution on a daily basis. The resulting product is made available through the GHRSST project and can be downloaded from the PO.DAAC website at: https://podaac.jpl.nasa.gov/dataset/CMC0.1deg-CMC-L4-GLOB-v3.0. For more details please refer to Brasnett (2008).

3.3. Operational Sea Surface Temperature and Ice Analysis (OSTIA)

The Operational Sea Surface Temperature and Ice Analysis (OSTIA) system is run by the UK's Met Office (Good et al., 2020). OSTIA provides daily gap-free maps of foundation SST with a horizontal resolution of 0.05° × 0.05°, using in-situ and satellite data from both IR (AVHRR, Visible-Infrared Imager-Radiometer Suite, Geostationary Operational Environmental Satellites_IMAGER and Spinning Enhanced Visible and Infra-Red Imager) and MW radiometers (AMSR2, TRMM Microwave Imager, Special Sensor Microwave Imager/Sounder and SSM/I) provided by the GHRSST project. The OSTIA reanalysis we use in this study is the near real time version 2 distributed by Copernicus Marine Environment Monitoring Service (CMEMS) https://data.marine.copernicus.eu/product/SST_GLO_SST_L4_NRT_OBSERVATIONS_010_001/description (last accessed on 31 October 2023).

3.4. Climate Change Initiative (CCI)

The second version (2.1) of the European Space Agency (ESA) Climate Change Initiative (CCI) data set offers global daily estimates of SST derived from observations captured by various IR sensors, including AVHRR, Advanced Along Track Scanning Radiometer, and Sea and Land Surface Temperature Radiometer. These CCI SST estimates aim to provide a consistent and reliable climate data record with minimal bias. The data set comprises cohesive maps of daily average SST on a $0.05° \times 0.05°$ grid, effectively filling in data gaps through optimal interpolation. The ESA SST CCI L4 analyses were generated using the OSTIA system (Good et al., 2020). This data set is made available through CMEMS and can be accessed at https://data.marine.copernicus.eu/product/SST_GLO_SST_L4_REP_OBSERVATIONS_010_024/description (last accessed on 31 October 2023). For more details please refer to Merchant et al. (2019).

3.5. MUR

A GHRSST L4 analysis of SST is produced as a retrospective data set (with a 4-day delay) and a near-real-time data set (with a 1-day delay) at the "PO.DAAC." This analysis is performed using wavelets as basis functions within an optimal interpolation framework on a global grid with a resolution of 0.01°. The Version 4 Multiscale Ultrahigh Resolution (MUR) L4 analysis is built upon nighttime GHRSST observations acquired from various instruments, including MW radiometers such as AMSR-E, AMSR2, WindSat, as well as IR radiometers like MODerate-resolution Imaging Spectroradiometer and AVHRR. In situ SST observations from the NOAA iQuam project are also incorporated. Ice concentration data obtained from the archives at the European Organization for the Exploitation of Meteorological Satellites Ocean and Sea Ice Satellite Application Facility High Latitude Processing Center are utilized to enhance SST parameterization in high-latitudes. Alongside SST, the data set includes additional variables for certain granules, such as SST anomaly derived from a MUR climatology and the temporal proximity to the nearest IR measurement for each pixel. The initial funding for this data set was provided by the NASA MEaSUREs program, and it is currently supported by the PO.DAAC. It is distributed as part of the GHRSST project through the PO.DAAC website at https://podaac.jpl.nasa.gov/dataset/MUR-JPL-L4-GLOB-v4.1. For more details please refer to Chin et al. (2017).

4. Methods

We computed the singularity exponents at the resolution scale using the equation

$$h(\vec{x}) \approx \frac{\log|\overline{\nabla T}|_\ell - \log\langle|\overline{\nabla T}|_\ell\rangle}{\log(\ell/\ell_0)} + \mathcal{O}\left(\frac{1}{\log(\ell/\ell_0)}\right), \tag{6}$$

where d is the dimension of the space; $\langle\cdot\rangle$ stands for the spatial mean; and

$$\frac{\ell}{\ell_0} = \frac{1}{(N_{\max})^{\frac{1}{d}}}, \tag{7}$$

with $N_{\max}$ being the number of observations, is the quotient between the resolution scale and the integral scale (Turiel et al., 2006). Notice that, the error in the estimation of the singularity exponents depends on the number of observations as $(d \log N_{\max})^{-1}$, which implies that a minimum number of observations are needed to keep the errors in the method small. As a rule of thumb, Pont et al. (2013) propose that the number of observations should be $N_{\max} > 100^d$, which is true for all the analyzed data sets. In this study, the coarse-grained thermal gradients of Equation 6 were obtained using the filtering method proposed by Pont et al. (2013). The above equation was applied to each daily SST map of every data set (see Figure 1). Then, the singularity spectrum of each snapshot of SST singularity exponents was computed using the histogram method (easily derived from Equation 5),

$$D(h_i) \approx d - \frac{\log N_i - \log N_{\max}}{\log(\ell/\ell_0)}, \tag{8}$$

where N_i is the number of grid cells having a singularity exponent in the range $\left[h_i - \frac{\delta h}{2}, h_i + \frac{\delta h}{2}\right)$ and $\ell/\ell_0 = \left(\sum_i N_i\right)^{-\frac{1}{d}}$. We discarded the grid points surrounding the land mask to avoid spurious values due to the

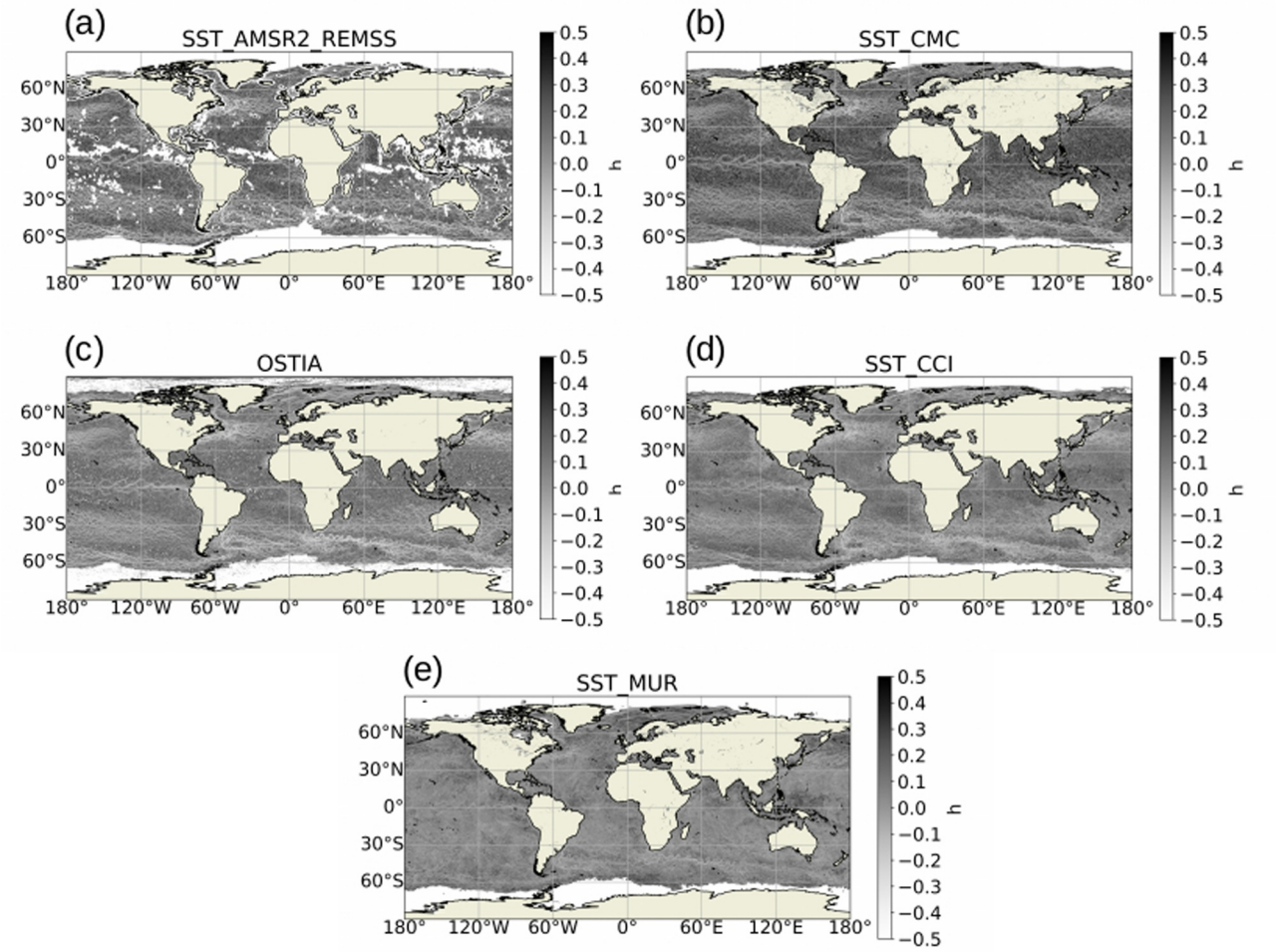

Figure 1. Example of singularity exponents for a daily sea surface temperature (SST) image corresponding to the 29 September 2016 for: (a) Advanced Microwave Scanning Radiometer 2_Remote Sensing Systems (AMSR2_REMSS), (b) Canadian Meteorological Center (CMC), (c) Operational Sea Surface Temperature and Ice Analysis (OSTIA), (d) Climate Change Initiative (CCI) and (e) Multiscale Ultrahigh Resolution (MUR).

land-sea transition and we used $d = 2$ and $\delta h = 0.08$ in the range from $h = -1$ to $h = 3$ for computing $D(h)$. Translational invariance was imposed on each singularity spectrum in order to correct for any shift that may exist in the singularity exponents (Turiel et al., 2006). Invariance was achieved by requiring that $\langle |\overline{\nabla T}|_\ell \rangle$ does not depend on the scale ℓ.

5. Results

We observe in Figure 1 that the patterns of SST singularity exponents are similar for all of the data sets, with the possible exception of MUR. The most intense thermal fronts, brighter lines in the figure associated with the smaller singularity exponents, are located in the most dynamical and frontally rich regions, such as the western boundary currents (Gulf Stream, Kuroshio, Agulhas) or the equatorial and antarctic circumpolar currents. Figure 2 shows the singularity exponents for the Agulhas current region to facilitate the comparison between the data sets. The spatial pattern of the most intense SST fronts are similar for all of the data sets. However, the singularity exponents of the most intense thermal fronts obtained for the SST MUR are higher (less brighter) than the ones of the rest of data sets, indicating that the intensity of thermal fronts in the SST MUR data set is lower compared to the other data sets.

We computed the singularity spectrum $D(h)$ (Equation 8) for each daily SST map in each of the data sets (Figure 3). Since all data sets attempt to reproduce the same field, we should expect the same singularity spectrum for all data sets regardless of their spatial resolution because the singularity spectrum is independent of the scale.

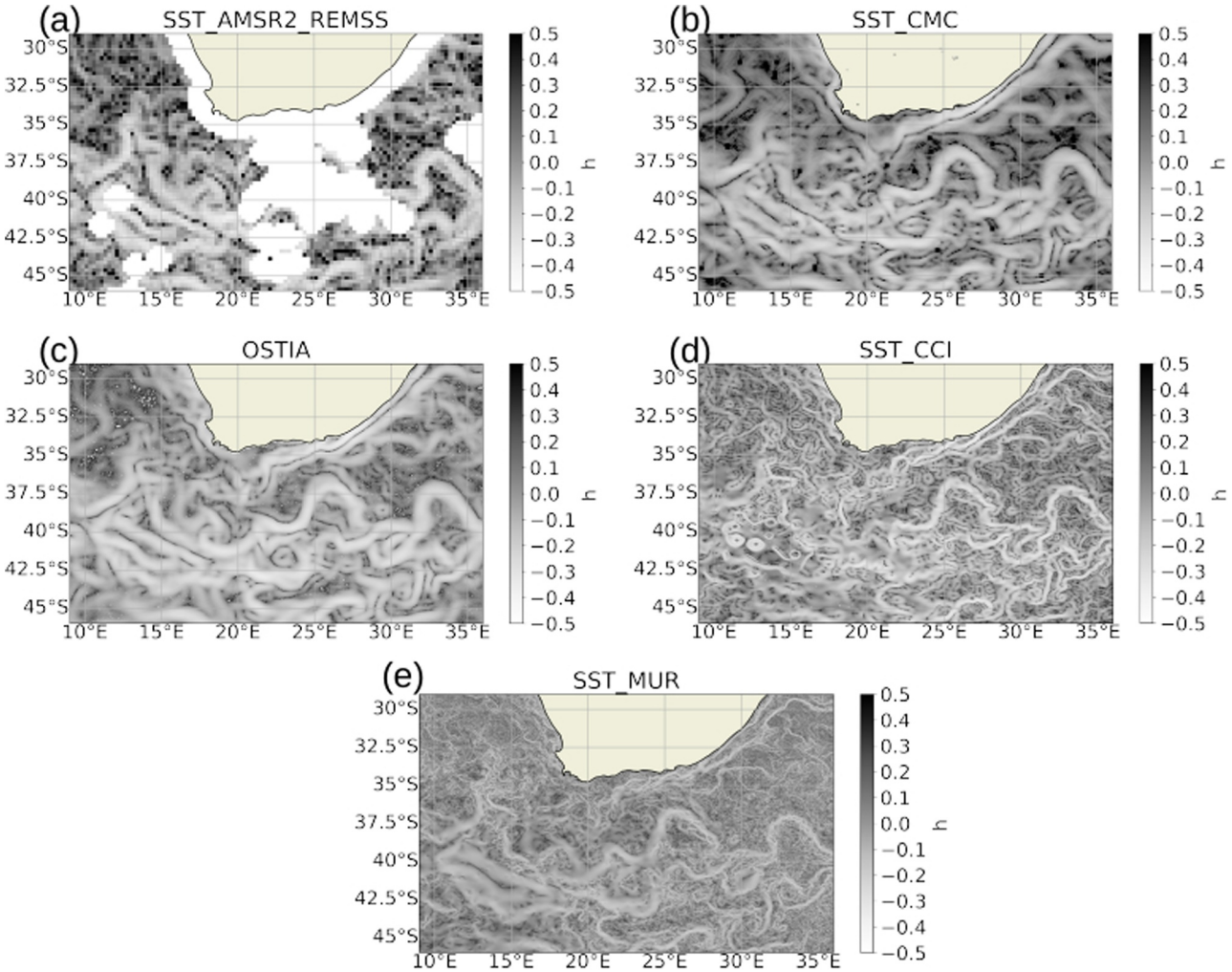

Figure 2. Example of a daily sea surface temperature (SST) singularity exponents for the Agulhas region corresponding to the 29 September 2016 (same as in Figure 1) for: (a) Advanced Microwave Scanning Radiometer 2_Remote Sensing Systems (AMSR2_REMSS), (b) Canadian Meteorological Center (CMC), (c) Operational Sea Surface Temperature and Ice Analysis (OSTIA), (d) Climate Change Initiative (CCI) and (e) Multiscale Ultrahigh Resolution (MUR).

This scale independence of the singularity spectrum and the analysis of the scales for which microcanonical multifractal holds for SST has been shown previously in Isern-Fontanet et al. (2007). However, since the new diagnostic we propose here is based on this statement and in order to make this paper self-contained, we have include a figure to illustrate the singularity analysis applied to the same AMSR-E SST image at different resolution scales: 0.25° (the nominal resolution), 0.5° and 1° (see Figure 4). We obtained the same structures and values for the singularity exponents with coarser resolution as we degrade them. The gaps of missing data of the singularity exponents are larger as we degrade the scale since we discard the adjacent pixels of missing data before computing the gradient. The singularity spectrum for all the scales considered is the same (Figure 4d), illustrating its scale invariant property.

The singularity spectra for the four L4 SST data sets, shown in Figure 3, deviate from the expected concave singularity spectrum obtained for the L3 SST_AMSR2_REMSS data set (red lines in Figure 3). Of the L4 data sets, MUR presents the closest behavior to the expected concave distribution given by the L3 SST AMSR-E REMSS. However, it shows a narrower overall range, defined as the difference between the largest and smallest singular values. This confirms that the amplitude of the most intense fronts are underestimated, as seen in the example of the Agulhas region (Figure 2). The singularity spectra of the remaining three data sets (CMC, CCI and OSTIA) deviate significantly from an expected smooth concave curve for exponents larger than order 0.3. The

10.1029/2023EA003088

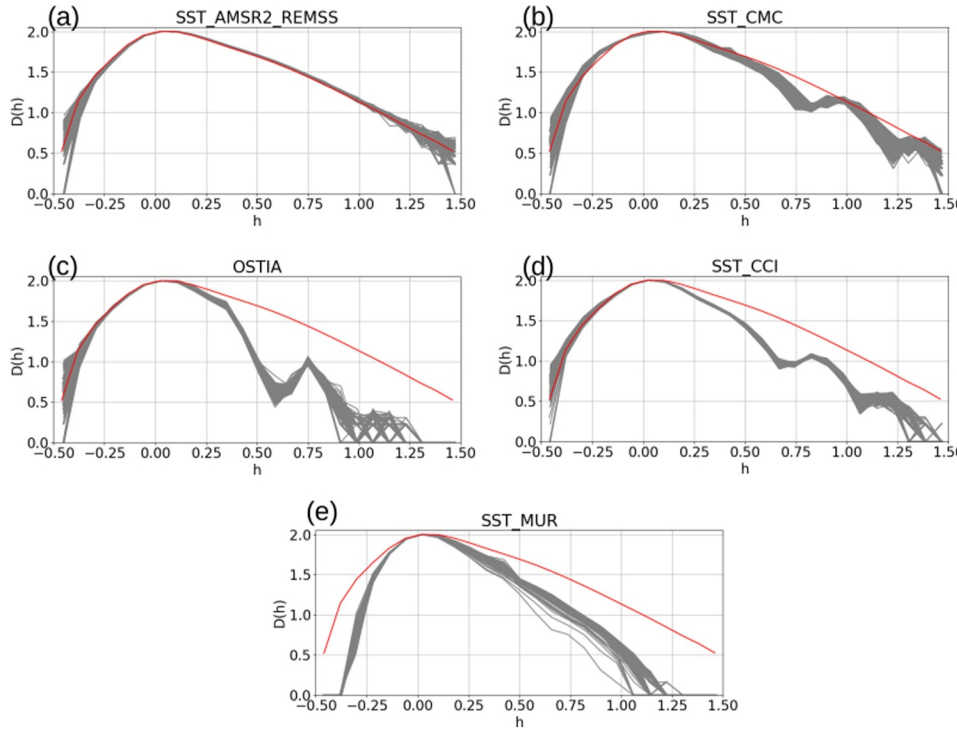

Figure 3. Singularity spectra $D(h)$, each gray line corresponds to a daily singularity spectrum of sea surface temperature (SST) for: (a) Advanced Microwave Scanning Radiometer 2_Remote Sensing Systems (AMSR2_REMSS), (b) Canadian Meteorological Center (CMC), (c) Operational Sea Surface Temperature and Ice Analysis (OSTIA), (d) Climate Change Initiative (CCI) and (e) Multiscale Ultrahigh Resolution (MUR). The red line corresponds to the median of the AMSR2_REMSS singularity spectra.

large dips in D(h), such as the one at 0.6 in the OSTIA spectrum, indicate an unexpected loss of energy in the associated product at the corresponding scales.

To better understand the loss of energy in the 0.3–0.6 range of the singularity spectrum of the OSTIA product, we computed the fraction of days for which the singularity value fell within this range. For comparison we include the same fraction for the AMSR2 data set for which the shape of D(h) is closest to that expected (Figure 5). The most striking differences are observed in the center of the large subtropical gyres, where the energy is relatively low compared with that of frontal regions associated with strong open ocean currents, such as the Gulf Stream and Kuroshio, following separation from the continental margin, or the Antarctic Circumpolar Current. These regions of strong currents are characterized by the most negative singular values (Figures 1 and 2) and, as expected, correspond to regions of lower probability for intermediate singular exponents (white regions in Figure 5 for the AMSR2 data set). The probability of intermediate singular values in the subtropical gyres for the OSTIA data set is much lower than expected based on the AMSR2 data set. This may be due to smoothing by the L4 algorithms in these regions, resulting in a more homogeneous SST than expected and the consequent loss of spatial structure and energy.

In order to investigate whether the loss of energy or the smoothing of SST gradients is caused by the L4 algorithms, we reinterpolated the OSTIA SST product to a 0.25° grid and repeated the analysis. As shown in Figure 6, the singularity spectrum $D(h)$ for the reinterpolated SST is closer to the expected concave shape given by AMSR2_REMSS and it no longer shows the significant dip in intermediate singularity exponents (0.3–0.6). In addition, the probability of having singularity exponents in that range has increased in the center of the large subtropical gyres with respect to the original higher spatial resolution data set shown in Figure 5b. These results further support the suggestion above that the interpolation system used in the L4 algorithm to fill the gaps in SST observations and blend different SST observations is losing structural information found in the actual SST fields.

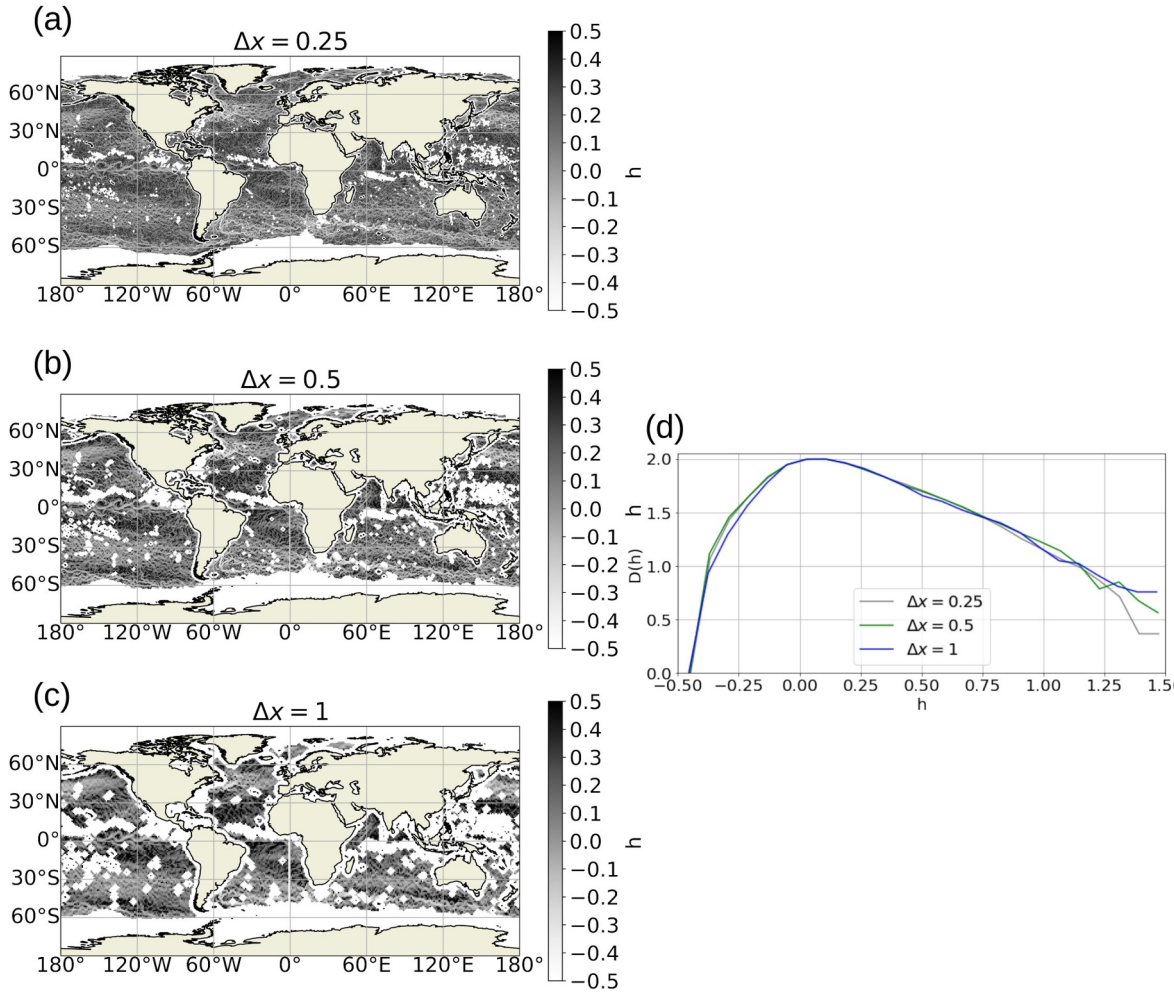

Figure 4. Example of singularity exponents for the same global Advanced Microwave Scanning Radiometer 2_Remote Sensing Systems (AMSR2_REMSS) sea surface temperature (SST) image corresponding to the 29 September 2016 at different resolution scales: (a) 0.25° (original grid), (b) 0.5° and (c) 1°, (d) singularity spectrum for each resolution: 0.25° (gray), 0.5° (green), 1° (blue).

6. Discussion

We propose here an approach to assess and intercompare SST products from a dynamical and structural perspective. The method is based on the multifractal theory of turbulence and consists in computing the singularity spectrum of SST singularity exponents. The singularity exponents represent the geometrical projection of the turbulence cascade and its singular spectrum can be seen as the probability density function of the singularity exponents normalized by the scale. Departures of the observed singularity spectra from their expected theoretical concave shape suggest limitations of the SST products to properly reproduce dynamical features in the SST fields; for example, smoothing of intermediate SST gradients in the OSTIA product located mostly in the subtropical gyres. We showed that this distortion may be caused by the different algorithms used to produce the gap-free L4 SST products.

Indeed, most SST retrievals are designed for global accuracy and are not designed to preserve under all observation scenarios the full amplitude of SST contrasts associated with submesoscale to mesoscale features in the near-surface SST fields (Merchant et al., 2009). Most of the algorithms retrieving SST from brightness temperatures are designed to minimize the SST error variance across some relatively large scales. However, what controls the ability to reproduce changes of SST at small scales is given by the sensitivity of brightness temperature to SST.

10.1029/2023EA003088

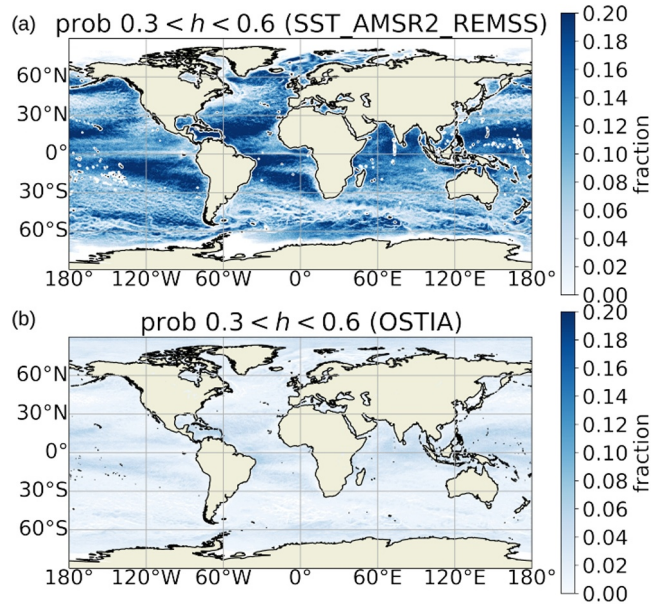

Figure 5. Fraction of days per year (2016) for which the singularity exponents are in the range [0.3, 0.6], in which the singularity spectra departs from the expected behavior (see Figure 3) for: Advanced Microwave Scanning Radiometer 2_Remote Sensing Systems (AMSR2_REMSS) (a) and Operational Sea Surface Temperature and Ice Analysis (OSTIA) (b).

The MUR data set is the L4 product with the most concave singularity spectrum (Figure 3). This data set is based on the Multi-Resolution Variational Analysis (MRVA), with differences from the approaches used to produce the other L4 data sets that might result in better performance regarding the structural properties of the final SST fields. Although the MRVA method performs a weighted least-squares optimization similar to the objective interpolation commonly used to produce the other L4 products, it first decomposes the input data into additive components based on the spatial scale before data-fusion is performed independently for each of these scale components. It also uses multiple time scales; that is, a 5-day data window used for reconstruction of mesoscale features and data windows of only a few hours for the smaller scale features. Another attribute of MRVA that may have a big impact in preserving the characteristics of SST fronts is that it is a mesh-less interpolation method, preserving the original measurement coordinates without resorting to a pre-gridding procedure such as nearest grid-point interpolation (Chin et al., 2017).

In addition to gap-filling methods, interactions between SST sampling regimes and aspects of geophysical variability may influence the singularity spectra. In particular, the MUR data set uses only night-time SST inputs, whereas others use day and night data. Geophysical variability that differentially affects the surface expression of dynamically driven gradients may therefore contribute to the contrast between MUR and others. Near-surface diurnal warming occurs in areas of light winds and strong insolation, and it is observed that in such conditions the surface warm layers tend to mask the underlying mixed-layer temperature gradients (Katsaros & Soloviev, 2004; Katsaros et al., 2005). We note that the observed smoothing effect causing non-concave spectra is contributed to strongly by the sub-tropical gyres, where conditions can be favorable for diurnal warm layer formation (Gentemann et al., 2008), suppressing gradients observable in day time SSTs. In that regard, OSTIA and CMC L4 pre-processing SST systems reject all daytime SST observations for surface winds under 6 m/s to produce estimates of "Foundation SST," so it seems unlikely that diurnal warming affects CMC, OSTIA or MUR. Further research should assess whether this contributes to the differences between analyses significantly.

Our results suggest that in order to produce coherent L4 SST fields with the turbulent characteristics of the oceanic flow, the interpolation schemes used should take into account the multiplicative cascade properties.

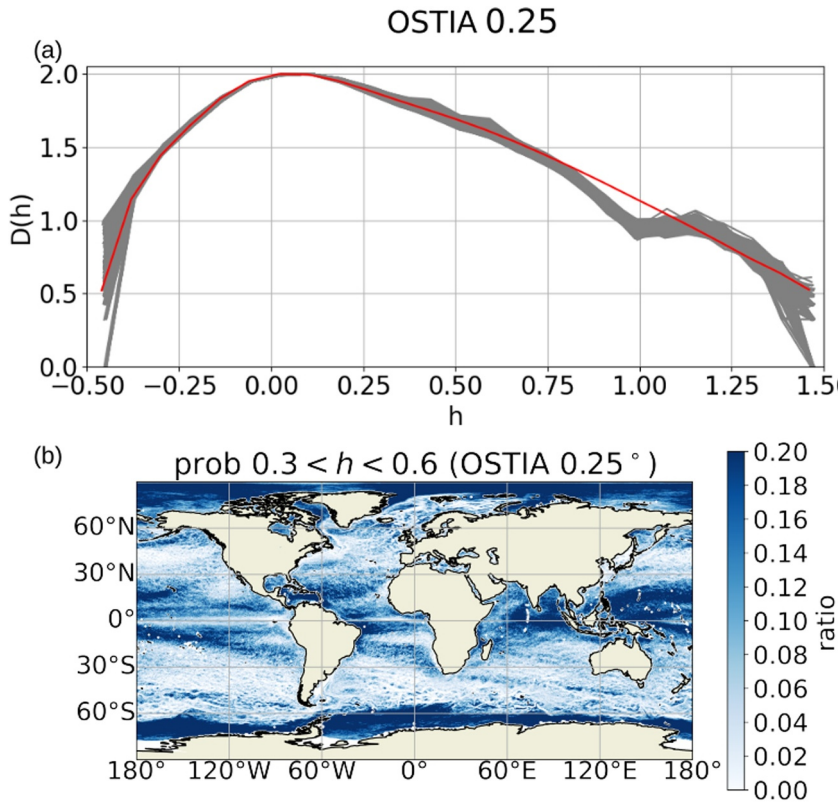

Figure 6. (a) Singularity spectra D(h) for the reinterpolated Operational Sea Surface Temperature and Ice Analysis (OSTIA) sea surface temperature (SST) (each gray line corresponds to a daily singularity spectrum of SST). (b) Fraction of days per year (2016) for which the singularity exponents are in the range [0.3, 0.6] for the reinterpolated OSTIA SST (as in Figure 5).

7. Conclusion

We proposed a new approach based on the multifractal theory of turbulence for assessing SST products from a dynamical and structural perspective. We showed that the evaluation of the singularity spectrum of SST singularity exponents and its departure from the predicted behavior allows us to assess the different limitations of each SST product. Particularly, we found that most of the data sets analyzed tend to smooth intermediate SST gradients typically allocated in the subtropical gyres regions. It appears that the sampling properties of the input SST products and the methodologies for gap filling are not capable of reflecting the full structural information of SST for the full range of spatial scales on which L4 analysis is attempted. Open questions remain about how deviations from the expected concave structure of the singularity spectrum relate to the methodological choices of producers. Further work needs to be done in that direction to find a combination of quantitative metrics for intercomparing the singularity spectrum of each data set.

Reproducing the multiplicative cascade of turbulence in the final L4 SST products is a key aspect from a dynamical point of view, and for related applications such as front and eddy detection, among others. Further work needs to be done to improve interpolation schemes to obtain more realistic SST products. Since the singularity spectrum is scale invariant, the new interpolation schemes could use a multi-scale approach by imposing the singularity spectrum given by the coarser resolution SST observation from MW radiometers.

Acronyms

AATSR	Advanced Along Track Scanning Radiometer
ACC	Antarctic Circumpolar Current
AMSR2	Advanced Microwave Scanning Radiometer 2

AMSR-E	Advanced Microwave Scanning Radiometer—EOS
AVHRR	Advanced Very High Resolution Radiometer
CCI	Climate Change Initiative
CMC	Canadian Meteorological Center
CMEMS	Copernicus Marine Environment Monitoring Service
ECV	Essential Climate Variable
ESA	European Space Agency
EUMETSAT	European Organization for the Exploitation of Meteorological Satellites
GCOM-W1	Global Change Observing Mission—Water
GHRSST	Group for High Resolution Sea Surface Temperature
GOES	Geostationary Operational Environmental Satellites
ICOADS	International Comprehensive Ocean-Atmosphere Data Set
iQuam	In situ SST Quality Monitor
IR	Infrared
L3	Level-3
L4	Level-4
MEaSUREs	Making Earth System data records for Use in Research Environments
METOP-A	Meteorological Operational satellite-A
METOP-B	Meteorological Operational satellite-B
MMF	Multifractal Microcanonical Formalism
MODIS	MODerate-resolution Imaging Spectroradiometer
MRVA	Multi-Resolution Variational Analysis
MUR	Multiscale Ultrahigh Resolution
NASA	National Aeronautics and Space Administration
NOAA	National Oceanic and Atmospheric Administration
OI	objective interpolation
OSI SAF	Ocean and Sea Ice Satellite Application Facility
OSTIA	Operational Sea Surface Temperature and Ice Analysis
PDF	probability density function
PO.DAAC	Physical Oceanography—Distributed Active Archive Center
REMSS	Remote Sensing Systems
SEVIRI	Spinning Enhanced Visible and Infra-Red Imager
SLSTR	Sea and Land Surface Temperature Radiometer
SSM/I	Special Sensor Microwave/Imager
SSMI/S	Special Sensor Microwave Imager/Sounder
SST	sea surface temperature

TMI	TRMM Microwave Imager
UK	United Kingdom
VIIRS	Visible-Infrared Imager-Radiometer Suite

Data Availability Statement

Four different L4 SST GHRSST formatted data set (CMC, OSTIA, CCI and MUR) and a L3 SST provided by REMSS were used in the creation of this manuscript. All data sets are publicly available from the original data providers:

- REMSS (Wentz et al., 2021) [Dataset] from https://data.remss.com/amsr2/ocean/L3/, accessed on 11 August 2022.
- CMC (Brasnett, 2008) [Dataset] from https://podaac.jpl.nasa.gov/dataset/CMC0.1deg-CMC-L4-GLOB-v3.0, accessed on 11 August 2022.
- OSTIA (Good et al., 2020) [Dataset] from https://data.marine.copernicus.eu/product/SST_GLO_SST_L4_NRT_OBSERVATIONS_010_001/description
- CCI (Merchant et al., 2019) [Dataset] from https://data.marine.copernicus.eu/product/SST_GLO_SST_L4_REP_OBSERVATIONS_010_024/description
- MUR (Chin et al., 2017) [Dataset] from https://podaac.jpl.nasa.gov/dataset/MUR-JPL-L4-GLOB-v4.1.

The SST derived singularity exponents [Dataset] described in Section 4 are available in https://doi.org/10.20350/digitalCSIC/15293 (González-Haro et al., 2022). The software used to process the data are available at González-Haro and Isern-Fontanet (2023). Figures were made with Matplotlib version 3.3.4 (Caswell et al., 2020; Hunter, 2007), available under the Matplotlib license at https://matplotlib.org/. Maps were created using Cartopy, released under a LGPL license with a shared copyright model at https://scitools.org.uk/cartopy/docs/latest/index.html (Met Office, 2010–2015). Input and output netCDF files were read and created, respectively, using xarray version 0.16.0 available at https://docs.xarray.dev/en/stable/ under the Apache License, Version 2.0 (the "License") (Hoyer & Hamman, 2017).

Acknowledgments
This work was supported by the INTERACT project, Grant PID2020-114623RB-C31, and the DEMON project, Grant PID2021-123457OB-C21, both funded by MICIU/AEI/10.13039/501100011033 and ERDF/EU. This work was also supported by the European Maritime, Fisheries and Aquaculture Fund (EMFAF). This work also acknowledges the ''Severo Ochoa Centre of Excellence'' accreditation, Grant CEX2019-000928-S funded by MICIU/AEI/10.13039/501100011033. This work is moreover a contribution to CSIC PTI Teledetect. The authors would like to thank Helen Beggs, J. Xavier Prochaska and another anonymous reviewer for their valuable comments during the revision process.

References

Arneodo, A., Bacry, E., & Muzy, J. F. (1995). The thermodynamics of fractals revisited with wavelets. *Physica A: Statistical Mechanics and Its Applications*, *213*(1), 232–275. https://doi.org/10.1016/0378-4371(94)00163-N

Beggs, H. (2010). Use of TIR from space in operational systems. In *Oceanography from space: Revisited* (pp. 249–271).

Beggs, H. (2021). Temperature. In *Earth observation: Data, processing and applications. Volume 3b: Applications—Surface waters*. Cooperative Research Centre for Spatial Information (CRCSI). Ch 14.

Brasnett, B. (2008). The impact of satellite retrievals in a global sea-surface-temperature analysis. *Quarterly Journal of the Royal Meteorological Society*, *134*(636), 1745–1760. https://doi.org/10.1002/qj.319

Caswell, T. A., Droettboom, M., Lee, A., Hunter, J., Firing, E., Sales De Andrade, E., et al. (2020). matplotlib/matplotlib: Rel: v3. 3.1. *Zenodo*.

Chelton, D. B., & Wentz, F. J. (2005). Global microwave satellite observations of sea surface temperature for numerical weather prediction and climate research. *Bulletin America Meteorology Social*, *86*(8), 1097–1116. https://doi.org/10.1175/BAMS-86-8-1097

Chin, T. M., Vazquez-Cuervo, J., & Armstrong, E. M. (2017). A multi-scale high-resolution analysis of global sea surface temperature. *Remote Sensing of Environment*, *200*, 154–169. https://doi.org/10.1016/j.rse.2017.07.029

Dash, P., Ignatov, A., Martin, M., Donlon, C., Brasnett, B., Reynolds, R. W., et al. (2012). Group for high resolution sea surface temperature (GHRSST) analysis fields inter-comparisons—Part 2: Near real time web-based Level 4 SST quality monitor (L4-SQUAM). *Deep Sea Research Part II: Topical Studies in Oceanography*, *77*, 31–43. https://doi.org/10.1016/j.dsr2.2012.04.002

Deser, C., Alexander, M. A., Xie, S.-P., & Phillips, A. S. (2010). Sea surface temperature variability: Patterns and mechanisms. *Annual Review of Marine Science*, *2*(1), 115–143. https://doi.org/10.1146/annurev-marine-120408-151453

Donlon, C. J., Casey, K. S., Robinson, I. S., Gentemann, C. L., Reynolds, R. W., Barton, I., et al. (2009). The GODAE high-resolution sea surface temperature pilot project. *Oceanography*, *22*(3), 34–45. https://doi.org/10.5670/oceanog.2009.64

Eyink, G. L. (2005). Locality of turbulent cascades. *Physica D: Nonlinear Phenomena*, *207*(1), 91–116. https://doi.org/10.1016/j.physd.2005.05.018

Fiedler, E. K., Mao, C., Good, S., Waters, J., & Martin, M. (2019). Improvements to feature resolution in the OSTIA sea surface temperature analysis using the NEMOVAR assimilation scheme. *Quarterly Journal of the Royal Meteorological Society*, *145*(725), 3609–3625. https://doi.org/10.1002/qj.3644

Fiedler, E. K., McLaren, A., Banzon, V., Brasnett, B., Ishizaki, S., Kennedy, J., et al. (2019). Intercomparison of long-term sea surface temperature analyses using the GHRSST multi-product ensemble (GMPE) system. *Remote Sensing of Environment*, *222*, 18–33. https://doi.org/10.1016/j.rse.2018.12.015

Frisch, U. (1995). *Turbulence: The legacy of A.N. Kolmogorov*. Cambridge Univ. Press.

Gentemann, C. L., Minnett, P. J., Le Borgne, P., & Merchant, C. J. (2008). Multi-satellite measurements of large diurnal warming events. *Geophysical Research Letters*, *35*(22), L22602. https://doi.org/10.1029/2008gl035730

GHRSST Project Office, Beggs, H., Karagali, I., & Castro, S. (2023). Sea surface temperature: An introduction to users on the set of GHRSST formatted products [Computer software manual]. https://doi.org/10.5281/zenodo.7589540

González-Haro, C., & Isern-Fontanet, J. (2023). cgharo/sst_singularity_analysis: Initial release. *Zenodo*. https://doi.org/10.5281/zenodo.8081159

González-Haro, C., Isern-Fontanet, J., & Turiel, A. (2022). SST singularity exponents v1.0 [Dataset]. *BEC, ICM-CSIC*. https://doi.org/10.20350/digitalCSIC/15293

Good, S., Fiedler, E., Mao, C., Martin, M. J., Maycock, A., Reid, R., et al. (2020). The current configuration of the OSTIA system for operational production of foundation sea surface temperature and ice concentration analyses. *Remote Sensing*, *12*(4), 720. https://doi.org/10.3390/rs12040720

Heygster, G., Kachi, M., Kelly, R., & Liu, G. (2017). Guest editorial the global change observation mission-water: Contributions to global water cycle science from the advanced microwave scanning radiometer-2. *IEEE Journal of Selected Topics in Applied Earth Observations and Remote Sensing*, *10*(9), 3835–3838.

Hoyer, S., & Hamman, J. (2017). xarray: Nd labeled arrays and datasets in python. *Journal of Open Research Software*, *5*(1), 10. https://doi.org/10.5334/jors.148

Hunter, J. D. (2007). Matplotlib: A 2D graphics environment. *Computing in Science & Engineering*, *9*(03), 90–95. https://doi.org/10.1109/mcse.2007.55

Isern-Fontanet, J., Capet, X., Turiel, A., Olmedo, E., & González-Haro, C. (2022). On the seasonal cycle of the statistical properties of sea surface temperature. *Geophysical Research Letters*, *49*(8), e2022GL098038. https://doi.org/10.1029/2022GL098038

Isern-Fontanet, J., & Turiel, A. (2021). On the connection between intermittency and dissipation in ocean turbulence: A multifractal approach. *Journal of Physical Oceanography*, *51*(8), 2639–2653. https://doi.org/10.1175/JPO-D-20-0256.1

Isern-Fontanet, J., Turiel, A., García-Ladona, E., & Font, J. (2007). Microcanonical multifractal formalism: Application to the estimation of ocean surface velocities. *Journal of Geophysical Research*, *112*(C5), C05024. https://doi.org/10.1029/2006jc003878

Kachi, M., Maeda, T., Tsutsui, H., Ono, N., Kasahara, M., & Mokuno, M. (2017). Five years observations of global water cycle by GCOM-W/AMSR2. In *2017 IEEE international geoscience and remote sensing symposium (IGARSS)* (pp. 5641–5643).

Katsaros, K. B., & Soloviev, A. V. (2004). Vanishing horizontal sea surface temperature gradients at low wind speeds. *Boundary-Layer Meteorology*, *112*(2), 381–396. https://doi.org/10.1023/b:boun.0000027905.90989.b2

Katsaros, K. B., Soloviev, A. V., Weisberg, R. H., & Luther, M. E. (2005). Reduced horizontal sea surface temperature gradients under conditions of clear skies and weak winds. *Boundary-Layer Meteorology*, *116*(2), 175–185. https://doi.org/10.1007/s10546-004-2421-4

Koutantou, K., Brunner, P., & Vazquez-Cuervo, J. (2023). Validation of NASA Sea Surface Temperature satellite products using Saildrone data. *Remote Sensing*, *15*(9), 2277. https://doi.org/10.3390/rs15092277

Lovejoy, S., Currie, W., Tessier, Y., Claereboudt, M., Bourget, E., Roff, J., & Schertzer, E. (2001). Universal multifractals and ocean patchiness: Phytoplankton, physical fields and coastal heterogeneity. *Journal of Plankton Research*, *23*(2), 117–141. https://doi.org/10.1093/plankt/23.2.117

Martin, M., Dash, P., Ignatov, A., Banzon, V., Beggs, H., Brasnett, B., et al. (2012). Group for high resolution sea surface temperature (GHRSST) analysis fields inter-comparisons. Part 1: A GHRSST multi-product ensemble (GMPE). *Deep Sea Research Part II: Topical Studies in Oceanography*, *77*, 21–30. https://doi.org/10.1016/j.dsr2.2012.04.013

Meneveau, C., & Sreenivasan, K. (1991). The multifractal nature of turbulent energy dissipation. *Journal of Fluid Mechanics*, *224*, 429–484. https://doi.org/10.1017/s0022112091001830

Merchant, C., Embury, O., Bulgin, C. E., Block, T., Corlett, G. K., Fiedler, E., et al. (2019). Satellite-based time-series of sea-surface temperature since 1981 for climate applications. *Scientific Data*, *6*(1), 1–18. https://doi.org/10.1038/s41597-019-0236-x

Merchant, C., Harris, A., Roquet, H., & Le Borgne, P. (2009). Retrieval characteristics of non-linear sea surface temperature from the advanced very high resolution radiometer. *Geophysical Research Letters*, *36*(17), L17604. https://doi.org/10.1029/2009gl039843

Met Office. (2010–2015). *Cartopy: A cartographic python library with a Matplotlib interface* (Tech. Rep.). Met Office. Retrieved from http://scitools.org.uk/cartopy

Muzy, J., Bacry, E., & Arneodo, A. (1994). The multifractal formalism revisited with wavelets. *International Journal of Bifurcation and Chaos*, *4*(2), 245–302. https://doi.org/10.1142/s0218127494000204

O'Carroll, A. G., Armstrong, E. M., Beggs, H., Bouali, M., Casey, K. S., Corlett, G. K., et al. (2019). Observational needs of sea surface temperature. *Frontiers in Marine Science*, *6*, 420. https://doi.org/10.3389/fmars.2019.00420

O'Neill, L. W., Esbensen, S. K., Thum, N., Samelson, R. M., & Chelton, D. B. (2010). Dynamical analysis of the boundary layer and surface wind responses to mesoscale SST perturbations. *Journal of Climate*, *23*(3), 559–581. https://doi.org/10.1175/2009JCLI2662.1

Perlin, N., de Szoeke, S. P., Chelton, D. B., Samelson, R. M., Skyllingstad, E. D., & O'Neill, L. W. (2014). Modeling the atmospheric boundary layer wind response to mesoscale sea surface temperature perturbations. *Monthly Weather Review*, *142*(11), 4284–4307. https://doi.org/10.1175/MWR-D-13-00332.1

Pont, O., Turiel, A., & Yahia, H. (2013). Singularity analysis of digital signals through the evaluation of their unpredictable point manifold. *International Journal of Computer Mathematics*, *90*(8), 1693–1707. https://doi.org/10.1080/00207160.2012.748895

Rayner, N. A., Brohan, P., Parker, D. E., Folland, C. K., Kennedy, J. J., Vanicek, M., et al. (2006). Improved analyses of changes and uncertainties in sea surface temperature measured in situ since the mid-nineteenth century: The HadSST2 dataset. *Journal of Climate*, *19*(3), 446–469. https://doi.org/10.1175/JCLI3637.1

Renault, L., Masson, S., Oerder, V., Jullien, S., & Colas, F. (2019). Disentangling the mesoscale ocean-atmosphere interactions. *Journal of Geophysical Research: Oceans*, *124*(3), 2164–2178. https://doi.org/10.1029/2018JC014628

Reynolds, R. W., Chelton, D. B., Roberts-Jones, J., Martin, M. J., Menemenlis, D., & Merchant, C. J. (2013). Objective determination of feature resolution in two sea surface temperature analyses. *Journal of Climate*, *26*(8), 2514–2533. https://doi.org/10.1175/jcli-d-12-00787.1

Robinson, I., Piollé, J.-F., LeBorgne, P., Poulter, D., Donlon, C., & Arino, O. (2012). Widening the application of AATSR SST data to operational tasks through the Medspiration Service. *Remote Sensing of Environment*, *116*, 126–139. (Advanced Along Track Scanning Radiometer (AATSR) Special Issue). https://doi.org/10.1016/j.rse.2010.12.019

Seuront, L., & Stanley, H. E. (2014). Anomalous diffusion and multifractality enhance mating encounters in the ocean. *Proceedings of the National Academy of Sciences*, *111*(6), 2206–2211. https://doi.org/10.1073/pnas.1322363111

Skákala, J., Smyth, T. J., Torres, R., Buckingham, C. E., Brearley, A., Hyder, P., & Coward, A. C. (2019). SST dynamics at different scales: Evaluating the oceanographic model resolution skill to represent SST processes in the southern ocean. *Journal of Geophysical Research: Oceans*, *124*(4), 2546–2570. https://doi.org/10.1029/2018JC014791

Sreenivasan, K. (1991). Fractals and multifractals in fluid turbulence. *Annual Review of Fluid Mechanics*, *23*(1), 539–604. https://doi.org/10.1146/annurev.fl.23.010191.002543

Turiel, A., Isern-Fontanet, J., García-Ladona, E., & Font, J. (2005). A multifractal method for the instantaneous evaluation of the stream-function in geophysical flows. *Physical Review Letters*, *95*(10), 104502. https://doi.org/10.1103/physrevlett.95.104502

Turiel, A., Pérez-Vicente, C. J., & Grazzini, J. (2006). Numerical methods for the estimation of multifractal singularity spectra on sampled data: A comparative study. *Journal of Computational Physics*, *216*(1), 362–390. https://doi.org/10.1016/j.jcp.2005.12.004

Turiel, A., Yahia, H., & Pérez-Vicente, C. J. (2008). Microcanonical multifractal formalism—A geometrical approach to multifractal systems: Part I. Singularity analysis. *Journal of Physics A: Mathematical and Theoretical*, *41*(1), 015501. https://doi.org/10.1088/1751-8113/41/1/015501

Wentz, F., Meissner, T., Gentemann, C., Hilburn, K., & Scott, J. (2021). *GCOM-W1 AMSR2 3-Day Environmental Suite on 0.25 deg grid, version 8.2* (Tech. Rep. No. Rpt. 05112021). Remote Sensing Systems. Retrieved from http://www.remss.com/missions/amsr/

Wick, G. A., Jackson, D. L., & Castro, S. L. (2023). Assessing the ability of satellite sea surface temperature analyses to resolve spatial variability–the northwest Tropical Atlantic atomic region. *Remote Sensing of Environment*, *284*, 113377. https://doi.org/10.1016/j.rse.2022.113377

Woo, H.-J., & Park, K.-A. (2020). Inter-comparisons of daily sea surface temperatures and in-situ temperatures in the coastal regions. *Remote Sensing*, *12*(10), 1592. https://doi.org/10.3390/rs12101592

Yang, C., Leonelli, F. E., Marullo, S., Artale, V., Beggs, H., Nardelli, B. B., et al. (2021). Sea surface temperature intercomparison in the framework of the Copernicus Climate Change Service (C3S). *Journal of Climate*, *34*(13), 5257–5283. https://doi.org/10.1175/jcli-d-20-0793.1